

Molecular Order of the Mesogens in Smectic Poly(ester imide) Fibers

Christoph Wutz,* Dagmar Gieseler, Tanja Maevis, and Norbert Stribeck

Institut für Technische und Makromolekulare Chemie, Universität Hamburg, Bundesstrasse 45, D-20146 Hamburg, Germany

Received December 4, 1998

ABSTRACT: The molecular order of the mesogens in the smectic liquid-crystalline (LC) and smectic-crystalline phases of different poly(ester imide)s (PEI) with similar chemical structure is investigated by means of X-ray fiber patterns. During the fiber spinning from the melt, the smectic LC phase is frozen. Above the glass transition temperature, a transition into a higher-ordered smectic-crystalline phase occurs. The PEI which are based on aminobenzoic acid trimellitimidate and long aliphatic spacers form exclusively orthogonal smectic phases (S_A , S_B , S_E). In contrast, the PEI based on aminocinnamic acid trimellitimidate and those derived from 4-hydroxyphthalic acid, aminophenol, and aliphatic dicarbon acids form tilted S_C phases. The layer line broadening of the X-ray reflections indicates a poor lateral order of the smectic layers in the LC phase due to a frequent inversion of the staggering direction between adjacent mesogens. As a result of the equatorial smearing of the four-point-pattern, the splitting angle of the reflections is not identical with the tilt angle between the mesogens and the normal of the smectic layer plane. The order of the mesogens in the direction perpendicular to the fiber axis is evaluated on the basis of the paracrystallinity model. The resulting local tilt angle corresponds to an average staggering amount of the mesogens. Furthermore, the parameter ϵ , introduced by Porod, is interpreted as a probability for the inversion of the staggering direction.

Introduction

Polymers with rigid and flexible segments in the main chain form very often liquid-crystalline (LC) phases and are, therefore, of technical and scientific interest. In the poly(ester imide)s (PEI) **1**, **2**, and **3** represented in Figure 1, the difference in the polarity between the aromatic mesogen and the aliphatic spacer is particularly large. Due to this amphiphilic character, these classes of polymers tend to form smectic layer structures. Determined by the length of the repeating unit, the d spacing of the smectic layers amounts to 20–40 Å and gives rise to reflections in the middle-angle X-ray scattering (MAXS, $2\theta = 1-5^\circ$). It should be emphasized that “smectic” is not synonymous with “liquid crystalline”. In addition to the smectic LC phases S_A and S_C a number of so-called higher-ordered smectic phases are reported, which are named S_B , S_E , S_F , or S_H and discriminated by the lateral order of the mesogens and their orientation with respect to the layer plane¹ (Figure 2). In contrast to low molar mass materials, for polymers these higher-ordered smectic phases are solid. Since the crystal-like packing of the mesogens results in additional reflections in the wide-angle X-ray scattering (WAXS, $2\theta = 5-40^\circ$), these phases are named “smectic crystalline” in this article. Nevertheless, the spacer segments exhibit a substantial conformational disorder,² in contrast to true three-dimensional crystal phases.

The phase behavior of the PEI **1**, **2**, and **3** has been investigated previously^{3,4} by differential scanning calorimetry (DSC), polarizing microscopy, and time-resolved X-ray scattering. Whereas the PEI **3** forms enantiotropic smectic LC phases, the monotropic, metastable LC phases of the PEI **1** and **2** occur exclusively upon cooling. During further moderate cooling, the LC phases transform into higher-ordered smectic-crystalline phases. Rapid quenching of the isotropic or LC melt below the glass transition temperature T_g yields a frozen smectic LC phase, a so-called smectic glass. Annealing above T_g causes again a transition into the higher-

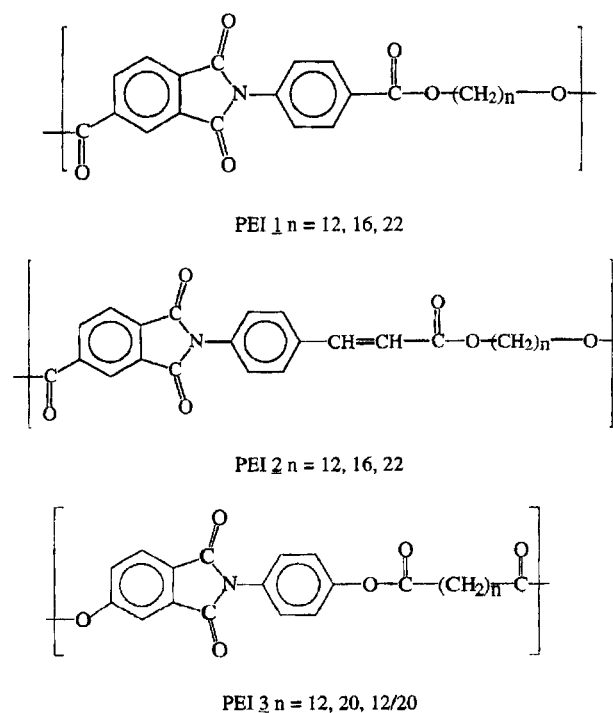


Figure 1. Chemical structure of PEI **1**, **2**, and **3**.

ordered phase. With increasing spacer length, the temperature interval of the LC phase becomes narrower, and in the cases of PEI **1** $n = 16, 22$ and PEI **3** $n = 20$ no LC phase exists at all. During the direct crystallization from the isotropic melt, spherulites grow which exhibit an internal smectic structure.^{5,6}

The acquisition of X-ray fiber patterns is well established as a method for the investigation of molecular order and orientation. In particular for side-chain and main-chain LC polymers, it represents a reliable means for the phase identification, because the microscopic texture is often disturbed and ambiguous. Several

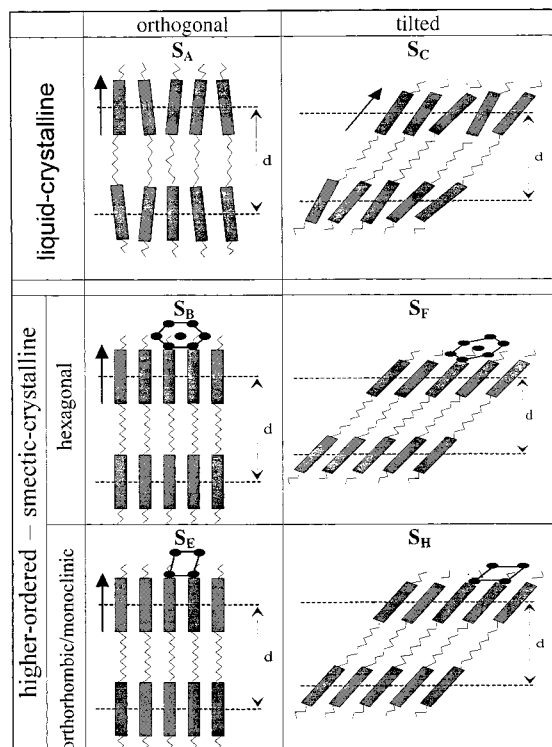


Figure 2. Schematic representation of the molecular order in different smectic phases.

authors⁷⁻¹¹ have demonstrated that the molecular order of the LC phase can be classified precisely by the position of the layer reflections in the MAXS and the azimuthal distribution of the WAXS. As a rule, the molecular chains are preferentially aligned parallel to the fiber axis, and the resulting WAXS exhibits intensity maxima located on the equator. In upright orthogonal smectic phases (S_A , S_B , S_E) the layer reflection in the MAXS occurs consequently at the meridian. In contrast, in tilted smectic phases (S_F , S_H , S_C) the layer normal forms an angle with the fiber axis, which results in an azimuthal splitting of the reflection. The splitting angle of the resulting four-point diagram β_{MAXS} corresponds to the tilt angle β_{SMECT} between the local director and the normal of the smectic layer plane. However, previous measurements have shown¹² that the meridional as well as the split MAXS reflections can exhibit a distinct horizontal broadening, which indicates a severe disturbance of the smectic layer order. In this case, it is questionable whether the splitting of the reflection can be interpreted as a tilt angle at all.

Layer line MAXS reflections have also been observed in the X-ray patterns of oriented nematic phases.^{8,13,14} In this case, a certain lateral order of the mesogens is achieved by application of an external magnetic or mechanical shear field. The lateral extension of the domains formed by correlated mesogens is on the order of only a few nanometers, which means that they form rather blocks or "cubes" than flatly extended layers. That is why this phase has been named cybotactic-nematic.¹⁵ However, the range of order should not affect the general classification of phases. Since these structures exhibit at least a short-range orientational order in the lateral direction, they should better be addressed as poorly ordered smectics.

Bar-shaped reflections have also been observed in the small-angle X-ray scattering (SAXS) patterns of semicrystalline polymer fibers. They result from a long-range

correlation among the domains in the direction parallel to the fiber axis and a rapid decay of correlation in perpendicular direction. Different theories and models^{16,17} have been developed to describe this phenomenon. In the following, we attempt to apply them to the evaluation and interpretation of the layer reflections from oriented, poorly ordered, smectic LC phases. The existence of layer line reflections in fiber diagrams has important implications on the MAXS of isotropic samples, too. Its effects on position and shape of isotropic MAXS reflections are discussed in a separate paper.¹⁸ On one hand, the relationship between the molecular structure and the resulting distribution of the scattering intensity is in principle the same for SAXS and MAXS, apart from the smaller particle size in the smectic structures which result in larger scattering angles. On the other hand, the principles of the structure formation are different in semicrystalline and smectic-LC systems, which results in a slightly different interpretation of the scattering data.

Experimental Section

Materials. All PEI samples studied have been synthesized in the group of Prof. H. R. Kricheldorf (Hamburg, Germany). The synthetic route and the basic properties of the polymers have been published previously.^{3,4} The polymers have been dissolved in a mixture of trifluoroacetic acid and CHCl_3 , precipitated into methanol and dried at 80 °C. Subsequently, fibers were drawn from the melt. Since the available amount of polymer is not sufficient for a continuous fiber spinning process, single fibers were drawn by hand. To avoid shrinking and loss of orientation, the fibers were annealed with fixed ends.

Measurements. The X-ray experiments were performed using the synchrotron radiation of the Deutsche Elektronen Synchrotron (DESY) in Hamburg, Germany, at a wavelength of $\lambda = 1.54 \text{ \AA}$. The time-resolved measurements of the MAXS and the WAXS were carried out simultaneously with two position-sensitive detectors and 30 s acquisition time per frame. The X-ray fiber patterns were recorded on image plates with an exposure time of 1–2 min. The fiber direction is vertical.

Results

The PEI **1** $n \leq 12$ display monotropic smectic LC phases, which undergo a transition into smectic-crystalline phases during further cooling. PEI **1** $n = 12$, for example, forms a S_A phase which transforms into a S_E phase upon moderate cooling. Rapid quenching of the isotropic or LC melt yields a frozen S_A phase, which during annealing above $T_g = 65 \text{ °C}$ forms first a metastable S_B phase and upon further heating above 110 °C the stable orthorhombic S_E phase. Figure 3a demonstrates the changes in the WAXS of quenched PEI **1** $n = 12$ during annealing. At ambient temperature, the amorphous halo of the S_A phase is slightly narrower than the halo of the isotropic melt. Above 65 °C a single reflection at $2\theta = 20^\circ$ develops, which is characteristic for the hexagonal ordered S_B phase. Above 110 °C a number of WAXS reflections occur that are attributed to the S_E phase. The development of the MAXS in Figure 3b shows that the layer reflection remains virtually at the same position, indicating a nearly constant layer spacing during the phase transitions. In all three phases (S_A , S_B , and S_E) the average direction of the mesogens and the spacers is oriented parallel to the normal of the layer planes, so that the d spacing corresponds to the length of the repeating unit. However, a closer analysis reveals slight changes in the

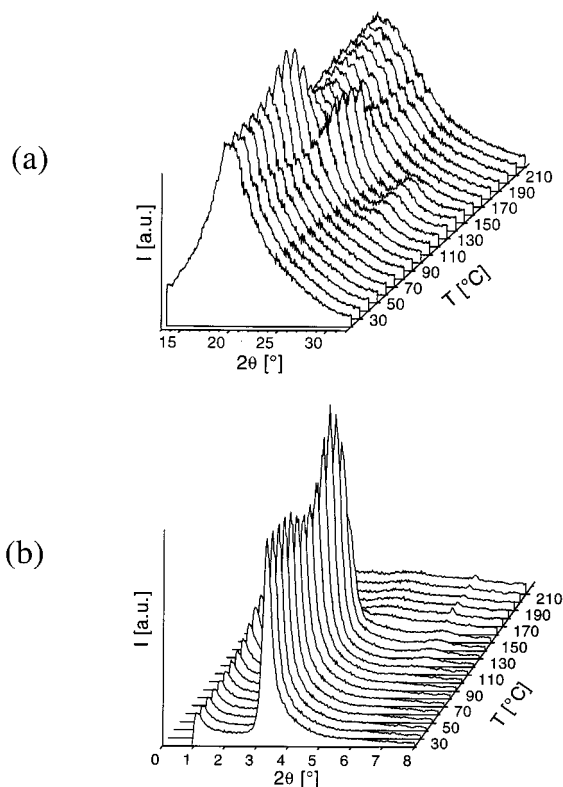


Figure 3. Change of WAXS (a) and MAXS (b) of quenched PEI **1** $n = 12$ during annealing.

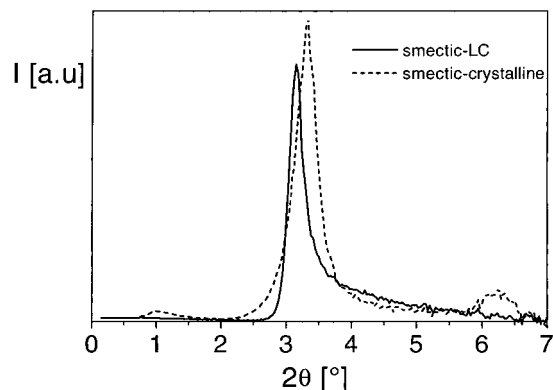


Figure 4. MAXS of PEI **1** $n = 12$ in the smectic LC phase (straight line) and in the smectic-crystalline phase (dotted line).

MAXS, which are clearly detectable in the comparison of the two single frames of the LC phase and the smectic-crystalline phase in Figure 4. First, the shape of the layer reflection in the LC phase is asymmetrical and exhibits a tail at larger scattering angles, while the peak of the crystalline phase is rather symmetrical. Second, the latter one exhibits a weak second-order reflection at $2\theta = 6.3^\circ$, which is not detectable in the LC phase. Nevertheless, the width of the reflection is narrower in the LC phase compared to the smectic-crystalline phase. Essentially the same characteristics of the reflections are found for the other samples.

The perpendicular orientation of the smectic layers with respect to the director becomes obvious in the X-ray fiber patterns. As an example, Figure 5 displays the MAXS of PEI **1** $n = 12$ fibers as drawn (a), after 15 min at 90°C (b) (S_E phase), and after 15 min at 135°C (S_E phase) (c). In all three cases the WAXS (not shown here) is located on the equator and the smectic layer reflection

occurs at $2\theta = 3.3^\circ$ on the meridian. The PEI **1** $n = 16$ and **22** exclusively form S_E phases which give rise to meridional layer reflections as well.

In contrast, for the PEI **2** $n = 12, 16,$ and **22**, a tilt of the mesogens relative to the normal of the layer plane and a staggering of adjacent repeat units occur during the transition from the LC phase into the smectic-crystalline (S_H) phase. As a consequence, the smectic layers become thinner and the MAXS reflection is shifted toward larger scattering angles. This effect can be observed in Figure 6, which shows the development of the MAXS of quenched PEI **2** $n = 12$ during heating at a rate of $10^\circ\text{C}/\text{min}$. In the beginning, the asymmetrical layer reflection of the frozen smectic LC phase is detected at $2\theta = 2.7^\circ$. Above $T_g = 65^\circ\text{C}$ it vanishes while the reflection of the S_H phase grows at $2\theta = 3.7^\circ$. More information about the order of the mesogens within the layers of different classes of smectic phases can be achieved from the X-ray patterns of macroscopically oriented samples. However, the investigation of an oriented LC melt is very difficult, since the X-ray scattering would have to be registered on-line during shear or fiber spinning. Both experiments would be costly and would need large amounts of polymer. Fortunately, the smectic LC phase can be frozen by rapid quenching below T_g for most of the samples, and this happens when a fiber is rapidly drawn from the melt. In this way, the molecular order and orientation of the LC phase can be studied on the solid fibers, if the absence of WAXS reflections indicates that crystallization was suppressed. By heating the fibers to temperatures above T_g , the transition into the oriented smectic-crystalline phase can be investigated as well.

Figure 7 shows the MAXS and WAXS of the PEI **2** $n = 12$ fiber as drawn (a) and after 15 min at 135°C (b). In both cases, the equatorial WAXS indicates that the molecules are oriented preferentially parallel to the fiber axis. The MAXS reflections are split into four maxima already in the frozen LC phase, indicating a S_C phase. From the connecting line between primary beam and scattering maximum an inclination angle of $\beta_{\text{MAXS}} = 23^\circ$ is determined with respect to the meridian. However, the reflections exhibit a strong layer line broadening, and the scattering intensity at meridian does not approximate zero at all. A number of higher-order reflections are detected at the meridian. Besides the second order, the fourth-order reflection exhibits considerable intensity.

Upon heating above T_g , the first-order MAXS reflections shift outward and the split angle β_{MAXS} increases to 38° . During this process, the reflections do not move by expanding a Debye circle but by increasing the spot distance parallel to the equator, while the component of the scattering angle in fiber direction remains constant. Finally, the reflections do not exhibit the layer line shape anymore, but their envelope becomes an ellipse. On one hand, the reflections have grown sharper perpendicular to the fiber direction; on the other hand, they are slightly broader in direction parallel to the fiber axis. A closer look at the MAXS reveals an additional weak layer line reflection at the meridian which indicates that a small fraction of the LC layer structure has persisted during crystallization.

For the PEI **2** $n = 16$, the LC phase cannot be frozen by the fiber spinning, because the crystallization proceeds much faster compared to $n = 12$ due to the prolongation of the flexible spacer. The splitting angle

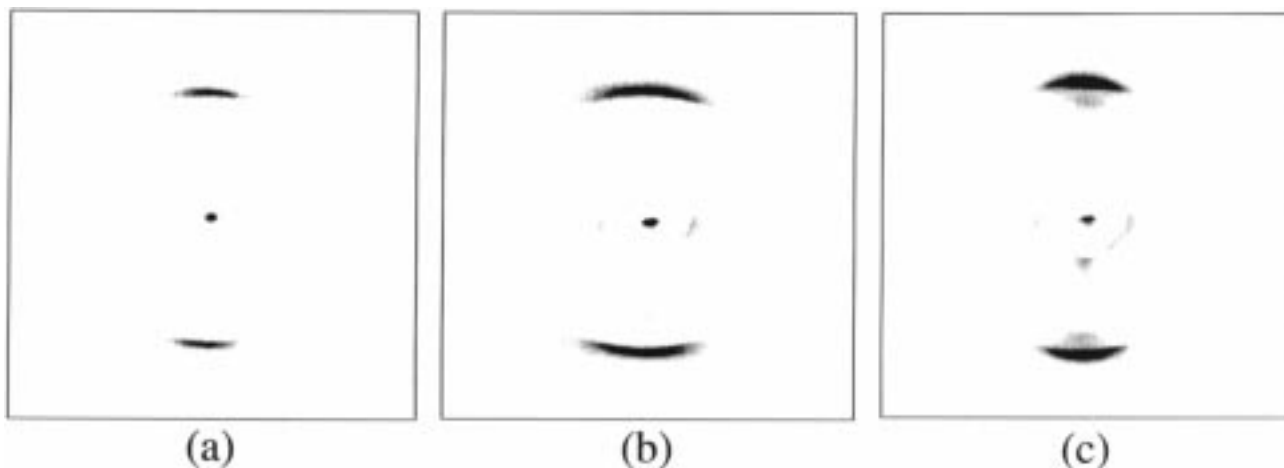


Figure 5. MAXS fiber patterns of PEI **1** $n = 12$ as drawn (a), after annealing at 90 °C for 15 min (b), and after 15 min at 135 °C (c).

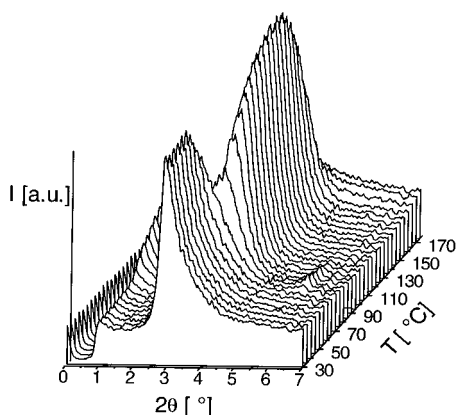


Figure 6. Change of the MAXS of PEI **2** $n = 12$ quenched from the melt during heating.

in the smectic-crystalline phase amounts to $\beta_{\text{MAXS}} = 37^\circ$. From the PEI **2** $n = 22$, unfortunately, no oriented samples could be obtained, neither by drawing nor by shearing. Probably, the further prolongation of the spacers increases the molecular mobility in a way that the orientation is lost by relaxation before the quenching freezes the molecular order.

From the PEI **3** materials, fibers could be drawn as well and studied by X-ray scattering. The pattern of the PEI **3** $n = 12$ as drawn fiber in Figure 8 clearly displays a split of the MAXS reflections into a four-point diagram with $\beta_{\text{MAXS}} = 50^\circ$. Once more, the reflections are broad in the horizontal direction, but the intensity at the meridian is much lower as compared to PEI **2** $n = 12$. In contrast, for PEI **3** $n = 14$ (Figure 9a) the reflection is more bar-shaped, and the split of the scattering maxima is smaller with a value of $\beta_{\text{MAXS}} = 37^\circ$. Remarkably, the second-, fifth-, and sixth-order reflections are arc-shaped and located on the meridian. After the thermal treatment (Figure 9b), a number of crystal reflections occur in the WAXS together with an intense layer reflection and a second-order reflection at the meridian of the MAXS. In addition, one observes four off-meridional, arc-shaped reflections which have the same meridional scattering angle than the first order of the meridional reflection. Furthermore, a small-angle X-ray scattering (SAXS) is detected at the meridian close to the beamstop. However, the interpretation of this SAXS is not the subject of this article.

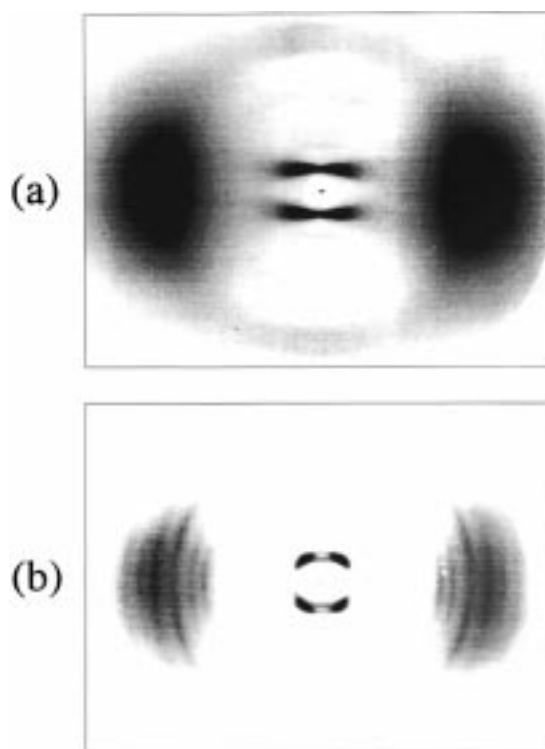


Figure 7. X-ray fiber patterns of PEI **2** $n = 12$ as drawn (a) and after 15 min at 135 °C (b).

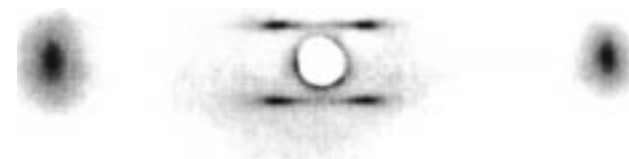


Figure 8. X-ray pattern of the PEI **3** $n = 12$ as drawn fiber.

The fibers of PEI **3** $n = 20$ exhibit a very poor orientation as observed previously for the other samples with the longest spacers. Nevertheless, a four-point diagram with a splitting of $\beta_{\text{MAXS}} = 65^\circ$ is detected in the MAXS shown in Figure 10a. The WAXS (not depicted) exhibits only one relatively sharp reflection at $2\theta = 20^\circ$. The combination of these reflections indicates a tilted hexagonal phase, e.g., S_F . Figure 10b depicts the MAXS fiber patterns after annealing at 135

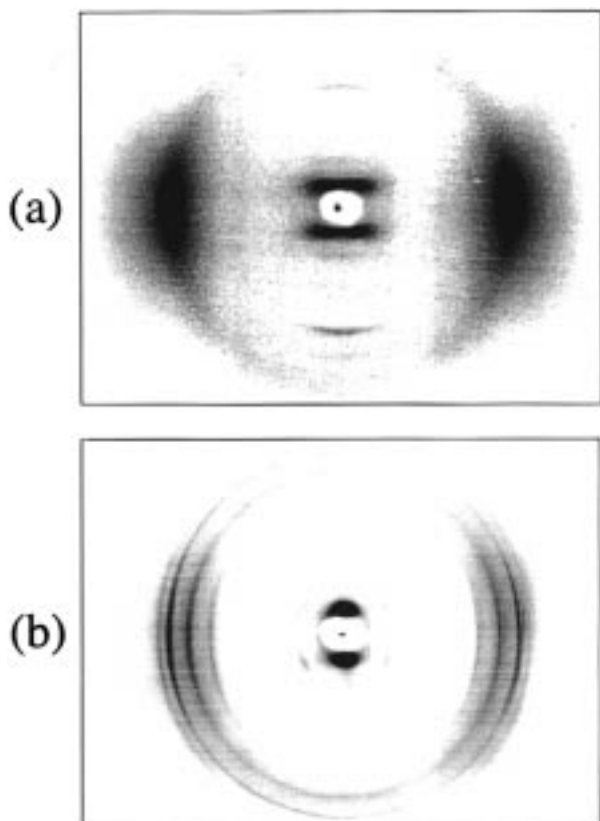


Figure 9. X-ray fiber patterns PEI **3** $n = 14$ as drawn (a) and after annealing at 135 °C (b).

°C for 15 min. In addition to the four-point diagram, a broad meridional reflection has occurred at a slightly lower scattering angle. In the WAXS, a number of equatorial crystal reflections occur indicating the S_E phase. The changes in the X-ray pattern are not due to a smectic–smectic phase transition but indicate a heterogeneous phase behavior of the sample. The S_E phase is formed at the expense of a nonlayered, probably nematic, phase.

The random copoly(ester imide) **3** $n = 12/20$ with an equimolar ratio of the two spacers exhibits a phase behavior that is similar to the $n = 12$ homopolymer. Previous investigations indicated, however, that the d spacing in the copolymer is increased in contrast to the homopolymer by the volume requirement of the docosane spacer. Figure 11 displays MAXS contour plots of a co-PEI **3** fiber during annealing. The frozen, oriented LC phase (at 50 °C) gives rise to a bar-shaped four-point pattern with $\beta_{\text{MAXS}} = 40^\circ$, similar to the homopolymer. Above T_g (100 °C), the reflections of the smectic-crystalline phase develop at a split angle of $\beta_{\text{MAXS}} = 10^\circ$. They are much more intensive and sharper in azimuthal direction than in the LC phase. During the transition one can see clearly that the reflections actually do not shift, but the inner reflections grow while the outer ones vanish. Less clearly this effect was detectable in the patterns of PEI **2** $n = 12$, because the change in the splitting was too small.

Discussion

The X-ray fiber patterns provide valuable information about the order and the orientation of the mesogens in different smectic phases. If extended layers can be assumed, the d spacing of the layers and their orientation with respect to the fiber axis can be calculated from

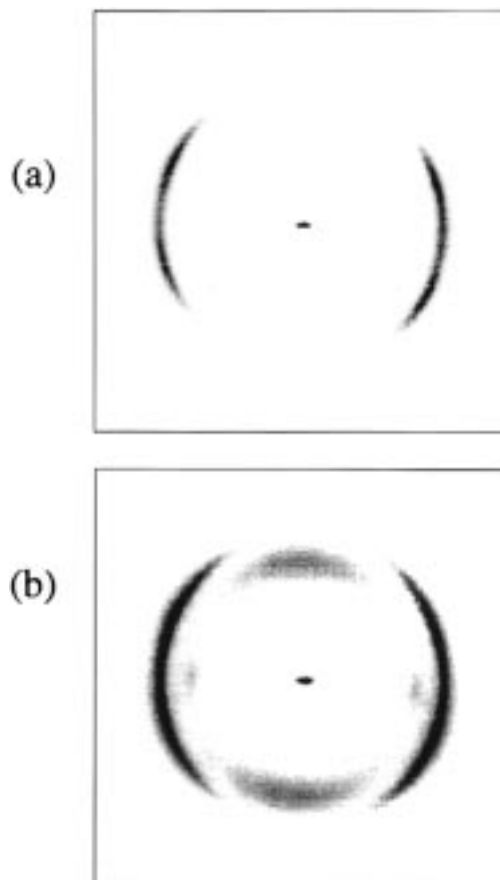


Figure 10. MAXS fiber patterns of PEI **3** $n = 20$ as drawn (a) and after 15 min at 135 °C (b).

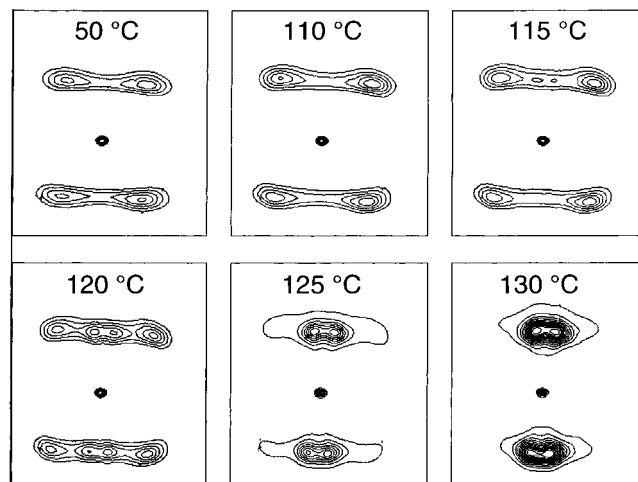


Figure 11. MAXS contour plots of a co-PEI **3** $n = 12/20$ fiber during annealing.

the positions of the MAXS reflections. From this, the orientation of the mesogens relative to the layer plane can be derived, provided that they are oriented preferentially parallel to the fiber axis. The latter assumption is fulfilled for all samples as indicated by the equatorial orientation of the WAXS, either halo or crystal reflections.

Other authors report on patterns in which the WAXS reflections are split azimuthally which indicates an inclination of the mesogens relative to the fiber axis,¹⁹ or the WAXS was located at the meridian and the MAXS reflection occurred at the equator due to an orientation of the smectic layers parallel to the fiber axis.²⁰ How-

Table 1. Spacing in Fiber Direction d_f , Lateral Spacing d_l , Porod Parameter ϵ , and Tilt Angle β in the Frozen LC Phases and in the Smectic-Crystalline Phases of Different PEI Samples As Determined from X-ray Fiber Patterns

sample	PEI 1		PEI 2		PEI 3		
	$n = 12$	$n = 16$	$n = 12$	$n = 16$	$n = 12$	$n = 14$	$n = 12/20$
frozen LC							
d_f [nm]	2.7	3.1	2.9		2.8	3.1	3.4
d_l [nm]			4.4		2.2	2.7	3.4
β [deg]	0	0	35		53	49	45
ϵ			-0.2		-0.5	-0.18	-0.25
crystalline							
d_f [nm] ^a	2.6	3.0	2.8	3.2	2.8	2.9	3.3
β [deg]	0	0	38	37	0	0	10

^a Measured at 135 °C.

ever, those results represent exceptions, and the latter case may be due to a low molecular weight or an orientation of not completely molten crystallites.

Furthermore, the shape of the MAXS reflections provides information on the quality of the layer formation. Since the reflections in the frozen smectic LC phase and the smectic-crystalline phase differ substantially in their shape, they are discussed separately in the following.

1. The Molecular Order of the Mesogens in the Oriented Frozen Smectic LC Phase. On one hand, the rate of crystallization is very low in the PEI (except for the longest spacers $n = 20, 22$), so that the crystallization is suppressed by rapid quenching below T_g . On the other hand, the formation of the LC phase is very fast, so that an oriented LC structure is frozen during fiber drawing from either the isotropic or the anisotropic melt. The powder patterns indicated, however, that the MAXS reflections are broader for a frozen smectic LC phase obtained by quenching the isotropic melt into ice-water, in contrast to the smectic melt. It can be concluded that the formation of the layers has been interrupted in an imperfectly ordered, intermediate stage during the quenching.

The MAXS reflections in the X-ray fiber patterns of the oriented, frozen smectic LC phase of the PEI **1**, **2**, and **3** exhibit three characteristic features: (i) either meridional orientation or a four-point splitting of the reflections; (ii) a layer line broadening of the reflections parallel to the equator; (iii) a low half-width in fiber direction. Since the vertical and horizontal intensity distribution exhibits characteristic differences, we decided to discuss the molecular order parallel and perpendicular to the fiber direction separately.

(a) Order in Fiber Direction. The MAXS reflections of the as-drawn fibers are relatively sharp in vertical direction which indicates a good correlation among the mesogens (layers) parallel to the fiber direction. That means the distance of the centers of gravity along the molecular chain is very uniform in the frozen LC phase. Since this distance depends on the length of the repeating unit and the length of the mesogen is virtually constant, the length of the spacers (thickness of the spacer layer) has to be rather uniform as well. This conclusion is supported by the conformational analysis of the spacer segments by means of ¹³C solid-state NMR. For the LC melt as well as for the frozen LC phase, a very uniform spacer conformation is found, which corresponds to the alternate-trans-model. It consists of a regular sequence of stable trans bonds alternating with disordered bonds which undergo rapid trans-gauche interconversions.^{2,21,22}

From the meridional component of the reflections scattering angle, a spacing of the smectic layers in fiber

direction d_f , corresponding to the length of the repeating unit, can be calculated via the Bragg equation. The resulting d_f values for all samples are listed in Table 1. As expected, d_f increases with the number of methylene groups in the spacer n and with prolongation of the mesogen (PEI **2** compared to PEI **1**). Previous studies indicated that an extrapolation to $n = 0$ gives a length for the pure mesogen which agrees very well with the results of computer modeling.⁴ The increase per methylene group amounts to approximately 1.1 Å, a value which fits exactly to the observed tg conformation.

The observation that the higher-ordered reflections are localized at the meridian of the fiber patterns, although the first order is split into a four-point diagram (Figures 7a and 9a), indicates a good correlation among the mesogens in fiber direction independent of their lateral ordering. Whereas the poor lateral order of the mesogens results in a rapid decay of the off-meridional scattering, the regular chemical structure of the main chain and its alignment parallel to the fiber axis form a rather perfect one-dimensional lattice which gives rise to first- and higher-order layer line reflections at the meridian.

Apart from the first and second order, the fourth order is the most intensive for PEI **1** and **2**, while for PEI **3** the fifth and sixth order exhibit the highest intensity. However, an evaluation of the form factor from the envelope is impossible, because at larger angles the tangent plane approximation is no longer valid. In the case of fiber symmetry this leads to a fundamental lack of information concerning the scattering intensity near the meridian of the representative plane in the reciprocal space.

(b) Order Perpendicular to the Fiber Direction. In the X-ray fiber diagrams of the PEI **1**, **2**, and **3**, the MAXS reflections of the oriented frozen LC phase exhibit a broad intensity distribution perpendicular to the fiber axis. In the S_C phase of PEI **2** and **3**, the reflections are split into a kind of four-point diagram. However, due to the severe horizontal broadening, one cannot assume flatly extended, smectic layers which incline certain angles with the fiber axis, because in this case the reflections would be sharp and oriented on a Debye circle. The question arises, in which way can the angle β_{MAXS} between the meridian and a connecting line between primary beam and the intensity maximum be interpreted?

As mentioned above, layer line-shaped MAXS reflections can result from nematic phases, if they are oriented macroscopically. Without any lateral correlation of the mesogens, the one-dimensional lattice gives rise to infinite layer lines parallel to the equator. In poorly ordered smectic phases, the lateral correlation

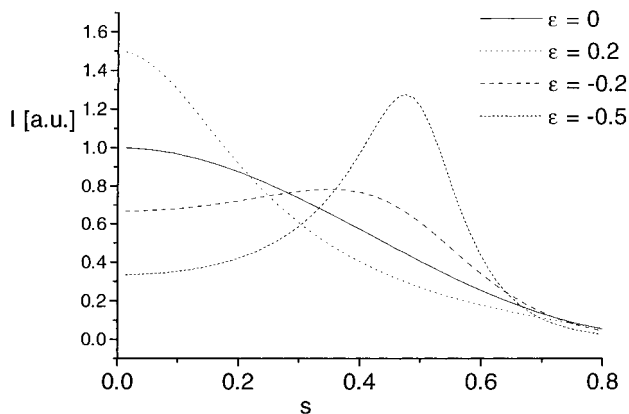


Figure 12. Influence of the Porod parameter ϵ on the scattering intensity distribution.

among the mesogens determines the equatorial width of the layer reflection.

The lack of periodicity in the direction perpendicular to the fiber axis indicates that a severely distorted two-dimensional paracrystalline lattice should be an adequate representation of this structure. The paracrystal model describes structures that exhibit only short-range order, but no long-range order.

In every lattice model, the scattering intensity is proportional to the product of the lattice factor $Z(s)$ and the square of the form factor $F(s)$:

$$I(s) \propto F(s)^2 Z(s) \quad (1)$$

where $s = 2 \sin \theta/\lambda$ is the absolute value of the scattering vector.

For square-shaped tiles with a length d and an excess electron density $\Delta\rho$, the form factor is given by¹⁶

$$F(s) = \Delta\rho d^2 \frac{\sin(\pi s d)}{\pi s d} \quad (2)$$

For systems with a poor correlation, Porod¹⁶ substituted the lattice factor by a correction factor $C(s)$, which considers the weak interaction between the particles.

$$C(s) = \frac{1 - \epsilon^2}{1 - 2\epsilon \cos(2\pi s d) + \epsilon^2} \quad (3)$$

ϵ is describing the "probability of contact" between neighboring particles. $\epsilon = -1$ corresponds to a perfect lattice, $\epsilon = 0$ is a random distribution, and $\epsilon > 0$ indicates clustering. In Figure 12 the influence of ϵ on the scattering curve is demonstrated theoretically. The curve passes through a maximum with increasing scattering angle already for a very poor correlation ($\epsilon = -0.2$). With decreasing perfection (increasing ϵ), the scattering maximum is shifted toward lower scattering angles. In the fiber diagram this effect corresponds to a decrease of the apparent splitting angle β_{MAXS} .

As an example, Figure 13 depicts a section through the four-point diagram in the X-ray fiber pattern of co-PEI **3** $n = 12/20$ parallel to the equator. The experimental scattering curve represented by symbols was fitted by the a calculated curve (solid line) based on eqs 1–3, giving an excellent agreement. In this case, we obtain values of $\epsilon = -0.25$ and $d = 1.67$ nm for the edge length of the tiles, which corresponds to the average cross section of a mesogen or spacer layer parallel to the equator. The distance between two mesogen blocks

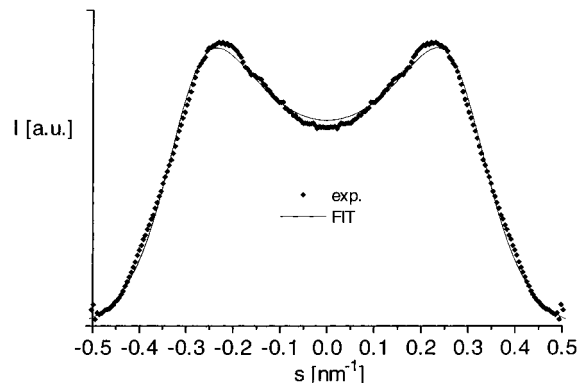


Figure 13. Scattering intensity of a cut parallel to the equator through the MAXS reflections of as drawn co-PEI **3** $n = 12/20$ fiber (Figure 11 top left) (symbols) and the best fit according to eqs 1–3 (straight line).

in this lateral direction d_l is given by

$$d_l = 2d \quad (4)$$

(c) Interpretation of ϵ and β . In the SAXS of semicrystalline fibers, bar-shaped reflections may result from a microfibrillar system. The scattering maximum occurs at the meridian in the case of $\epsilon \geq 0$, that is, if the fibrils are either distributed statistically or bundled. In contrast, a four-point diagram results from a lateral periodicity due to repulsive interactions among the domains of neighbored fibrils. On the basis of this model, Wunderlich et al.²³ have demonstrated that in PET fibers a third, noncrystalline, intermediate phase exists between the semicrystalline microfibrils.

At this point, we have to consider a difference between the interpretations of the four-point diagrams in the SAXS and those of the smectic LC phase, which is based on the different structural facts. In a semicrystalline fiber, the degree of crystallinity can vary largely, depending on the chemical structure of the polymer and the manufacturing process. Furthermore, the size distribution of the crystalline and amorphous regions is broad as a rule in both directions, parallel and perpendicular to the fiber axis. In contrast, in smectic LC polymers the regular length and sequence of polar, rigid mesogens and nonpolar, flexible spacers induce certain structural regularities. First, if the mesogens and spacers are approximately of the same length, half of the volume must be filled by mesogens, and no intermediate phase without mesogens can exist. Second, this class of segmented molecules tends to undergo a nanophase segregation due to the large difference in the polarities, and the resulting domains have a layered structure. Considering the observed scattering patterns, a probable notion of the structural morphology appears to be that of disturbed lamellae with nonperiodical undulations, as has been proposed by Bonart¹⁷ for semicrystalline polyethylene fibers. A schematic representation of such an irregularly undulated smectic layer system is depicted in Figure 14.

As a result of the periodical chemical structure and the macroscopic orientation, all mesogens are correlated in the direction of the fiber axis with the distance d_f , thus forming a one-dimensional lattice which gives rise to the observed reflection lines at the meridian. Due to the staggered arrangement of the mesogens and the tendency of forming layers, another mesogen domain is found in a distance d_l in lateral direction with a high

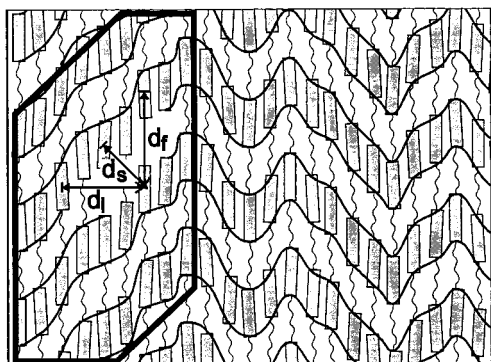


Figure 14. Schematic representation of an undulated smectic LC structure with a layer spacing in fiber direction d_f , in lateral direction d_l , and normal to the smectic layers d_s . The frame indicates the area with correlation among the layers normal to the mean layer plane.

probability (see Figure 14). However, in the LC phase the position and orientation of the mesogens fluctuate. During the quenching, the time-dependent fluctuations are frozen in, resulting in fluctuations in space. By this, the smectic layer obtains an irregular shape, and the lateral long-range order is lost.

Three effects have to be considered that weaken the lateral correlation among the mesogen domains. First, the longitudinal shift of a molecular chain may be so large that the correlation among the mesogens within the layer gets lost completely. Second, from the positional and orientational fluctuations of the mesogens, the smectic layers obtain a modulated shape. Due to this modulation, the layer spacings in lateral direction d_l as well as normal to the layer d_s (see Figure 14) exhibit a larger variation, and the off-meridional higher-order reflections are lost. More important is probably the third effect, that the direction of the staggering can be reversed. By this, the layer structure is conserved physically in the sense of phase segregation, but the layers obtain an irregularly undulated shape. The periodicity of mesogen and spacer blocks perpendicular to the fiber axis is lost, and the split MAXS reflections result only from the small parts of the layer structure between the staggering inversions (see Figure 14). The limited size of these blocks results also in a broader width of the split, off-meridional reflection compared to the meridional scattering. The asymmetrical chemical structure of the PEI mesogens may play an important role for this inversion of the staggering. The random distribution of head-to-head and head-to-tail connections along the chains induces an irregular arrangement of the mesogens with respect to their sense also in lateral direction.

The exploration of the scattering intensity distribution we proposed above allows a discrimination between the off-meridional scattering which originates from the domains with flat, tilted smectic layers and the smearing effect due to the undulations. From the molecular geometry of the domains with a correlated lateral d_l spacing and the layer thickness in fiber direction d_f , an angle $\beta_{\text{SMEC}} = \tan^{-1}(d_f/d_l)$ can be evaluated, which has to be interpreted only as an average angle between the fiber axis and the normal of a connecting line between the centers of gravity of two adjacent mesogens. The Porod parameter ϵ is responsible for the smearing of the scattering intensity due to the loss of lateral correlation among tilted smectic layers and, thus, may be interpreted as measure for the probability of

inversion of the staggering direction. A rare change of the staggering direction results in a good lateral correlation and ϵ values close to -1 ; a frequent, random inversion produces values close to zero. However, all three effects of disorder mentioned above influence the quantity of ϵ .

The results in Table 1 indicate that, for the three PEI 3 samples, the angles β_{SMEC} evaluated by the paracrystallinity model differ much less than the splitting angles of the MAXS reflections β_{MAXS} .

Furthermore, the repetition of the X-ray experiments with different fiber samples of the same charge of polymer indicates that the values of ϵ can vary by ± 0.1 , because the order of the smectic layers is obviously sensitive to the manufacturing parameters as melting temperature and spinning speed. In contrast, the values for d_l and accordingly for β_{SMEC} reproduce very well, because they depend only on the local order of adjacent mesogens and not on the long-range order.

At this point, we would like to emphasize that the observed molecular structure does not correspond to that of a $S_{\bar{A}}$ phase, which has been proposed for low molar mass and polymeric liquid crystals.^{24,25} While the $S_{\bar{A}}$ phase consists of an undulated, rippled arrangement of mesogen blocks with internal S_A order, the mesogens of the studied PEI are staggered with respect to each other and the undulations by inversion of the staggering direction are nonperiodical. In this respect, the observed structure could be addressed as S_C ; this is a layered structure with smectic-C-like fluctuations.

2. Mesogen Order in the Smectic-Crystalline Phase. During cooling of the LC phase or heating of the frozen LC glass, the development of crystal reflections in the WAXS indicates the transition into a higher-ordered smectic-crystalline phase. This process is accompanied by five characteristic changes of the MAXS reflections in the fiber or powder patterns: (i) the reflection intensity increases; (ii) the splitting angle β_{MAXS} changes (not for PEI 1); (iii) the half-width perpendicular to the fiber direction decreases; (iv) the reflections become slightly broader in fiber direction; (v) in addition to the meridional layer reflection, off-meridional arc-shaped reflections occur.

The increasing MAXS intensity can be explained by the fact that the molecular order is mainly improved within the mesogen layers, whereby the difference in the electron density between mesogen and spacer layer increases.

While the MAXS reflections of the PEI 1 remain at the meridian, the splitting angle β_{MAXS} changes during the crystallization of PEI 2 and 3. Since the reflections are sharp, β_{MAXS} is identical with the molecular tilt angle β_{SMEC} . The influence of the chemical structure on the tilt of the mesogens is discussed in the next section.

The MAXS reflections of the smectic LC phase and the smectic-crystalline phase are located on the same line parallel to the equator; i.e., the meridional component of the scattering angle remains invariable during the transition. From this observation, together with the equatorial position of the WAXS reflections, it can be concluded that the crystallization does not involve any tilting of the mesogens, but changes in the staggering which result in a reorientation of the smectic layers with respect to the fiber axis. In other words, the transition between the two smectic phases with different tilt angles is not induced by rotation of the mesogens but by longitudinal shifting of the mesogens which results

in a change of the inclination of the smectic layers with respect to the local director field.

The fiber patterns of co-PEI 3 $n = 12/20$ (Figure 11) indicate clearly that β_{MAXS} does not change continuously during the transition, but the LC reflections disappear while the reflections of the smectic-crystalline phase grow at a different position. Accordingly, the phase transition does not involve a continuous longitudinal reptation of the mesogens by a few angstroms, but a destruction of the LC layer order and a formation of new smectic-crystalline layers. However, the kinetics and the mechanism of this phase transition will be the subject of another publication in which we take into consideration the SAXS results as well.

The MAXS reflections in the smectic-crystalline phase are sharp. Therefore, the paracrystalline model does not need to be applied, but of course it is valid, resulting in ϵ values above 0.5. The position of the reflections can be evaluated simply via the Bragg equation.

The decreasing azimuthal half-width of the MAXS reflections clearly indicates an improvement of the layering during the crystallization. The layer structure is no longer a result of just the segregation, but it is based on strong enthalpic interactions between the mesogens. They are embedded into a crystal lattice so that the correlation within the layers cannot get lost easily by fluctuation anymore. Due to the regular arrangement of the mesogens, the boundary between mesogen and spacer layer becomes sharper so that second-order layer reflections are detected even in the powder patterns of unoriented samples. Furthermore, the X-ray fiber pattern of PEI 2 $n = 16$ exhibits the same splitting of first- and second-order reflection, which indicates a good correlation among tilted smectic layers.

In the fiber patterns of the orthorhombic, smectic-crystalline phases of PEI 1 and 3, four weak, arc-shaped, off-meridional reflections are observed on the same layer line as the meridional layer reflection. Since these reflections occur more or less pronounced in all samples with S_E structure and the crescents are not oriented on a Debye circle, the assumption of a second smectic-crystalline phase with a staggered arrangement (S_H) is ambiguous. Moreover, these reflections should be interpreted as a result of a lateral correlation among mesogen blocks which form a macrolattice. The model of a macrolattice has been proposed by Fronk and Wilke^{26,27} as a universal representation for the spatial distribution of crystallites in a semicrystalline fiber. On the basis of computer simulations, they have demonstrated that an orthorhombic macrolattice gives rise to a X-ray scattering in which $[h,0,1]$ reflections occur on a line parallel to the equator. For the smectic-crystalline structure the application of the model means that the smectic layers are separated periodically into blocks of mesogens. The reflections occur under an angle of $\theta_1 = 5^\circ$ relative to the meridian corresponding to a lateral block spacing of 17.6 Å, which is equivalent to four mesogens. This relatively small size of the crystals may be explained once more by the asymmetrical chemical structure of the mesogens and the random distribution of both orientation along the chain. Of course, the chains can undergo a longitudinal reptation until the fitting structures form a lateral order as has been proposed in non-periodic-layer crystals.²⁸ Or the required lateral order can be obtained by back-foldings of the chain. Whether the unit cell contains parallel or antiparallel packed mesogens is still ambiguous, because the deter-

mination of the crystal structure is still in progress. Anyway, the crystal size must be limited by the random mesogen sequence. On the other hand, the observed sharp reflections indicate fairly large crystals.

Despite the general increase of order, the MAXS reflections become slightly broader in meridional direction during the crystallization, indicating a deterioration of the long-range order among the smectic layers. A quantitative determination of the correlation length by the evaluation of the reflection width via Scherrer's equation will be published in a separate paper.¹⁸ However, since the thickness of the mesogen layer is uniform due to the regular mesogen packing, a larger variation in the thickness of the spacer layer has to be concluded. This conclusion is confirmed by the results of the conformational analysis of the spacer segments by ¹³C NMR CP/MAS on PEI 2 $n = 12, 16$.² As mentioned above, the spacers adopt a rather uniform alternate trans conformation in the LC phase. In contrast, the amounts of both ordered trans-trans sequences and completely disordered segments are increased in the smectic-crystalline phase, resulting in a nonuniform conformation. While the spacers play an important role in the layer formation by nanophase segregation in the fluid smectic phase, they are forced to adopt different conformations due to their attachment to the crystal-like packed mesogens in the smectic-crystalline phase.

3. Influence of the Chemical Structure on the Mesogen Orientation within the Smectic Layers.

The evaluation of the X-ray fiber patterns allows an unambiguous classification of the smectic phases formed by the PEI 1, 2, and 3. The tilt angles β listed in Table 1 confirm that the PEI 1 form exclusively upright smectic phase, whereas the LC phase in PEI 2 and 3 is tilted. In particular, the different molecular order in the LC phases of PEI 1 (S_A) and PEI 3 (S_C) cannot simply be explained by the geometry of the repeating unit, because the inversion of the carboxylate group does not change the direction of the spacer attachment. The same accounts for the double bond of the trans-substituted aminocinnamic acid in PEI 2 which causes only a slight side step.

For an average lateral mesogen distance of 4.4 Å, evaluated from the position of the WAXS halo, an average staggering quantity between adjacent mesogens in the LC phase can be calculated to be approximately 3 Å ($\beta_{\text{SMEC}} = 35^\circ$) for PEI 2 and 5.2 Å ($\beta_{\text{SMEC}} = 50^\circ$) for PEI 3.

A direct relationship between the tilt staggering of the mesogens in the LC phase and in the smectic-crystalline phase can also not be established. For PEI 2 $n = 12$, the splitting of the reflections β_{MAXS} increases during crystallization. However, the evaluation of β_{SMEC} indicated that the average staggering of the mesogens does not change virtually during the transition. In contrast, for the PEI 3, the tilt angle decreases to values close to zero. Consequently, one cannot assume that the staggering which exists in part or in average already in the LC phase becomes just uniform during the crystallization. Moreover, the free energy of the system is minimized in the LC phase by adopting a distinct average staggering quantity. In this process, the separation of polar and nonpolar segments and the minimization of the surface energy and the free volume are supposed to be the driving forces. In the smectic-crystalline phase, in contrast, a different, uniform

staggering exists due to the lateral dipole–dipole interactions between the mesogens. Which quantity of staggering results in the crystal structure with the lowest energy depends very sensitively on the chemical structure of the mesogens. The comparison of the β_{SMEC} values in Table 1 indicates that the tilt of the smectic-crystalline structure is independent of the spacer length. Furthermore, the WAXS reflections occur at the same position for each set of PEI with same mesogen but different spacer length. This observation indicates that the correlation of the WAXS among the smectic layers is lost due to the conformational disorder in such long spacers. Hence, crystalline order exists exclusively within the mesogen layer. The evaluation of the unit cells of PEI **1**, **2**, and **3** is in progress and not the subject of this article. However, we assume that the S_E phase formed by the PEI **1** corresponds to an orthorhombic crystal structure. For PEI **2**, the relatively low number of WAXS reflections indicates a monoclinic rather than a triclinic lattice, in which the tilt angle $\beta_{\text{SMEC}} \cong 36^\circ$ corresponds to an angle of $\beta + 90 = 126^\circ$ of the monoclinic unit cell.

In the fiber pattern of the co-PEI **3** $n = 12/20$ (Figure 11) we observed a tilt of 10° in the smectic-crystalline phase. In the patterns of the homopolymers $n = 12$ and 14 , this splitting could not be detected, maybe due to the poor orientation of the fibers. Since the WAXS reflections occur at the same positions for all three samples, the molecular order of the mesogens must be identical, namely a monoclinic unit cell with an angle of $\beta + 90^\circ = 100^\circ$.

The relationship between the chemical structure of the mesogens and their packing within the crystal could possibly be confirmed by molecular modeling using force field calculations, which however are expensive and have not been applied to these polymer systems yet.

Conclusions

By means of X-ray fiber patterns the molecular order of the mesogens in smectic phases can be determined in detail. The poly(ester imide)s **1**, **2**, and **3** form a variety of smectic phases dependent on the type of mesogen and the thermal treatment. The macroscopic orientation has no significant influence on the general phase behavior of the polymers. While the PEI **1** forms exclusively orthogonal smectic phase, the PEI **2** and **3** exhibit tilted smectic layers with a staggered arrangement of adjacent mesogens. The layer-line broadening of the split MAXS reflections in the oriented, frozen LC phase can be explained by the assumption of irregular undulations of the smectic layers. By an inversion of the staggering direction the extension of flat layers is restricted and the lateral correlation of the mesogen

domains is disturbed. The evaluation of the scattering intensity on a cut through the MAXS reflections parallel to the equator by the approach we adopted from Porod allows the independent determination of the average amount of staggering and tilting β between adjacent mesogens and a quantification of the undulations by the ϵ parameter.

Acknowledgment. The authors thank Prof. H. R. Kricheldorf for providing the PEI samples. X-ray investigations have been supported by HASYLAB Hamburg.

References and Notes

- (1) Gray, G. W.; Goodby, J. W. G. *Smectic Liquid Crystals*; Leonard Hill: New York, 1984.
- (2) Wutz, C.; Schleyer, D. *J. Polym. Sci., Part B: Polym. Phys.* **1998**, *36*, 2033.
- (3) Kricheldorf, H. R.; Probst, N.; Schwarz, G.; Wutz, C. *Macromolecules* **1996**, *29*, 4234.
- (4) Kricheldorf, H. R.; Probst, N.; Wutz, C. *Macromolecules* **1995**, *28*, 7990.
- (5) Wutz, C. *Polymer* **1998**, *39* (1), 1.
- (6) Wutz, C.; Schäfer, R. *Mol. Cryst. Liq. Cryst.*, in press.
- (7) Blumstein, A.; Vilasagar, S.; Ponrathnam, S.; Clough, S. B.; Blumstein, R. B. *J. Polym. Sci., Polym. Phys.* **1982**, *20*, 877.
- (8) Yoon, Y.; Ho, R.; Moon, B.; Kim, D.; McCreight, K. W.; Li, F.; Harris, F. W.; Cheng, S. Z. D.; Percec, V.; Chu, P. *Macromolecules* **1996**, *29*, 3421.
- (9) Watanabe, J.; Hayashi, M. *Macromolecules* **1988**, *21*, 278.
- (10) Shibaev, V. P.; Platé, N. A. *Adv. Polym. Sci.* **1984**, *60/61*, 173.
- (11) Nishikawa, E.; Finkelmann, H. *Macromol. Chem. Phys.* **1997**, *198*, 2531.
- (12) Wutz, C. *Mol. Cryst. Liq. Cryst.* **1997**, *307*, 175s.
- (13) Francescangeli, O.; Yang, B.; Laus, M.; Angeloni, A. S.; Galli, G.; Chiellini, E. *J. Polym. Sci., Part B: Polym. Phys.* **1995**, *33*, 699.
- (14) Li, M. H.; Brület, A.; Cotton, J. P.; Davidson, P.; Strazielle, C.; Keller, P. *J. Phys. II* **1994**, *4*, 1843.
- (15) DeVries, A. *Mol. Cryst. Liq. Cryst.* **1970**, *10*, 219.
- (16) Porod, G. *Mh. Chem.* **1972**, *103*, 395.
- (17) Bonart, R. *Kolloid Z. Z. Polym.* **1964**, *194* (2), 97.
- (18) Stribeck, N.; Wutz, C. *Macromolecules*, submitted.
- (19) Watanabe, J.; Hayashi, M.; Nakata, Y.; Niiri, T.; Tokita, M. *Prog. Polym. Sci.* **1997**, *22*, 1053.
- (20) Leland, M.; Wu, Z.; Chhajaj, M.; Ho, R.-M.; Cheng, S. Z. D.; Keller, A.; Kricheldorf, H. R. *Macromolecules* **1997**, *30*, 5249.
- (21) Leisen, J.; Boeffel, C.; Spiess, H. W.; Yoon, D. Y.; Sherwood, M. H.; Kawasumi, M.; Percec, V. *Macromolecules* **1995**, *28*, 6937.
- (22) Cheng, J.; Yoon, Y.; Ho, R.-M.; Leland, M.; Guo, M.; Cheng, S. Z. D.; Chu, P.; Percec, V. *Macromolecules* **1997**, *30*, 4688.
- (23) Fu, Y.; Annis, B.; Boller, A.; Jin, Y.; Wunderlich, B. *J. Polym. Sci., Polym. Phys.* **1994**, *32*, 2289.
- (24) Gane, P. A.; Leadbetter, J. *J. Phys. C* **1983**, *16*, 2059.
- (25) Davidson, P. A.; Keller, P.; Levelut, A. M. *J. Phys. (Les Ulis, Fr.)* **1985**, *46*, 939.
- (26) Fronk, W.; Wilke, W. *Colloid Polym. Sci.* **1983**, *261*, 1010.
- (27) Fronk, W.; Wilke, W. *Colloid Polym. Sci.* **1985**, *263*, 97.
- (28) Hanna, S.; Windle, A. H. *Polymer* **1988**, *29*, 207.

MA981891M